Average Sequential Water Molecule Binding Enthalpies of $M(H_2O)_{19-124}^{2+}$ (M = Co, Fe, Mn, and Cu) Measured with Ultraviolet Photodissociation at 193 and 248 nm

William A. Donald,[†] Ryan D. Leib,[†] Maria Demireva,[†] Bogdan Negru,[†,‡] Daniel M. Neumark,[†,‡] and Evan R. Williams*[,†]

Department of Chemistry, University of California, Berkeley, California 94720-1460, United States, and Chemical Sciences Division, Lawrence Berkeley National Laboratory, Berkeley, California 94720-8176, United States

Received: August 10, 2010; Revised Manuscript Received: November 18, 2010

The average sequential water molecule binding enthalpies to large water clusters (between 19 and 124 water molecules) containing divalent ions were obtained by measuring the average number of water molecules lost upon absorption of an UV photon (193 or 248 nm) and using a statistical model to account for the energy released into translations, rotations, and vibrations of the products. These values agree well with the trend established by more conventional methods for obtaining sequential binding enthalpies to much smaller hydrated divalent ions. The average binding enthalpies decrease to a value of ~10.4 kcal/mol for $n > \sim 40$ and are insensitive to the ion identity at large cluster size. This value is close to that of the bulk heat of vaporization of water (10.6 kcal/mol) and indicates that the structure of water in these clusters may more closely resemble that of bulk liquid water than ice, owing either to a freezing point depression or rapid evaporative cooling and kinetic trapping of the initial liquid droplet. A discrete implementation of the Thomson equation using parameters for liquid water at 0 °C generally fits the trend in these data but provides values that are ~0.5 kcal/mol too low.

Introduction

Interactions between ions and solvent molecules affect the stability, reactivity, and dynamics of ionic species in solution, particularly for reactions involving charge transfer or ion association, and these interactions play important roles in cellular function, protein crystallization, catalysis, radiolysis, and energy storage.[1,2] One approach to obtain information about ion−solvent interactions is to probe ions in a microsolvated environment, where the size and content of an individual cluster can be carefully controlled.[3−5] Information about how the physical properties of an ion in isolation evolve upon stepwise addition of solvent can be obtained and used to infer properties in bulk solution. Cluster measurements can be particularly important in cases where the lifetime of a charged particle, such as an electron in water,[6−14] is short, making condensed-phase measurements more difficult. Structural information can be obtained from spectroscopy[15−19] or can be inferred from trends in solvent binding energies measured as a function of cluster size.[20−36] Methods such as electrospray ionization[37] make it possible to experimentally investigate clusters with divalent[27,35] and even trivalent[38] ions, and new information about the structures and ion coordination numbers of these clusters containing multivalent ions is emerging.[15−17]

Several techniques have been used to measure sequential water molecule binding energies of hydrated divalent ions with up to 14 water molecules, including high-pressure ion source mass spectrometry (HPMS),[27,35,36] threshold collision-induced dissociation measurements (TCID),[31−34] and blackbody infrared radiative dissociation (BIRD).[28−30] These experiments show that the sequential binding enthalpies of a water molecule to a divalent ion depend on the ion identity and cluster size. The effects of metal ion identity are significant for smaller clusters that have relatively strong metal−ligand interactions but decrease rapidly with increasing cluster size as a result of increased ion solvation. For divalent Mg, Ca, Sr, and Ba, the thirteenth water molecule binding enthalpies range from 11.6 to 13.0 kcal/mol.[27]

Data for the sequential water binding energies to much larger cluster sizes are more limited, owing to the difficulty of applying many conventional thermochemical methods to large ions. Values for the sequential water molecule binding energies to $H^+(H_2O)_n$ (for n up to 28) were obtained from metastable decay measurements and ranged from 9 to 11 kcal/mol for n from 6 to 28.[25] These values are ~3.9 kcal/mol higher than those from collision-induced dissociation measurements, illustrating the difficulty of obtaining accurate data for large clusters.[26]

Another method to estimate ligand binding energies is to measure the number of ligands lost when an ionic cluster absorbs a photon of known energy.[39−41] Each molecule that is lost from the cluster after it absorbs a photon will remove energy corresponding to the binding energy and energy that is partitioned into translational, rotational, and vibrational energy of the products. Thus, the average energy removed per lost monomer, obtained by dividing the energy of the absorbed photon by the average monomer units lost, is an upper limit to the average sequential monomer binding energies of the lost monomers. Lineberger and co-workers measured the average number of CO_2 molecules lost when $(CO_2)_n^+$ and $(CO_2)_n^-$ absorb radiation at different wavelengths[26,27] and found that the average energy removed by each molecule was ~0.22 eV. A similar method was used to estimate the binding energy of water to $(H_2O)_{18}^-$ and $(H_2O)_{34}^-$ (~0.43 eV)[42] and hydrated cationized aniline, $An^+(H_2O)_n$, for n up to 20.[43] For $An^+(H_2O)_n$, the average energy removed per water molecule lost decreased from ~17.8 kcal/mol for $n = 5$ to a nearly constant value of ~9.7 kcal/mol

---

* To whom correspondence should be addressed. E-mail: Williams@cchem.berkeley.edu. Phone: (510) 643-7161. Fax: (510) 642-7714.

[†] University of California.

[‡] Lawrence Berkeley National Laboratory.

10.1021/jp107547r

for $n = 10-20$.[43] Because these later values are close to the binding energy of water to large ionic water clusters[44] and the bulk heat of vaporization (10.6 kcal/mol),[45] these data indicate that the energy of the absorbed photon is fully converted into internal energy of the precursor cluster. This is in contrast to recent UV photodissociation results for hydrated protonated proflavine, $PH^+(H_2O)_n$,[46] which indicate that full internal conversion, ion fluorescence, and formation of a long-lived triplet state can all occur when these clusters absorb a 248 nm photon.

Photodissociation experiments at 1064 nm have also been used to obtain the internal energy content of $(H_2O)_{48}^-$ and $(H_2O)_{118}^-$ and cluster heat capacities as a function of the initial ion temperatures.[42] The onset of sharp increases in the cluster heat capacities with increasing cluster temperature at 93 and 118 K, for $(H_2O)_{48}^-$ and $(H_2O)_{118}^-$, respectively, were attributed to the onset of cluster melting.[42] These results are consistent with the phenomenon of melting point depression, where particles melt at lower temperatures than the corresponding bulk material as the size of the particles decreases.

Cluster thermodynamics for sequential water molecule binding to large hydrated ions, which directly affect the lifetimes and stability of droplets, are important to modeling ion-induced nucleation,[47] obtaining cluster heat capacities from metastable decay measurements,[48] and ion nanocalorimetry.[13,14,46,49−58] The latter method, in which recombination energies (REs) of extensively hydrated ions are obtained from the number of water molecules lost upon electron capture, has been used to obtain values for the absolute potential of the standard hydrogen electrode (SHE) and absolute proton hydration energy.[49−51] In these experiments, a large number of water molecules can be lost from the reduced precursor. For example, electron capture by $Eu^{3+}(H_2O)_{103}$ results in reduction of Eu^{3+} and the loss of 15−19 water molecules.[49] The vast majority of the RE goes into breaking the binding interaction of the water molecules to the reduced precursor, which can be calculated using a discrete[44] implementation of the Thomson liquid drop model (TLDM).[44,59] Because of the large number of water molecules lost in these experiments, any systematic error in the calculated binding energy values is amplified by the number of water molecules lost. An alternative approach to obtain ion−electron REs is to measure the average number of water molecules lost upon deposition of a known amount of energy, such as upon the absorption of an UV photon, as a function of the energy deposited. By comparing the number of water molecules lost upon electron capture to absorption of different photon energies, the adiabatic REs of extensively hydrated ions can be experimentally determined. By combining these laser calibration experiments with our previous RE extrapolation method,[49] the absolute potential of the SHE and the absolute proton hydration energy could be obtained entirely from these experimental data.

Here, we report results from UV photodissociation of $M^{2+}(H_2O)_n$ (M = Co, Fe, Cu, Mn, and $CeNO_3$; $n \leq 124$), from which the average sequential water molecule binding enthalpies of extensively hydrated clusters can be obtained. These values indicate that the structure of water in these nanodrops may be more similar to that of bulk liquid water than ice and that values calculated from the TLDM are slightly too low for clusters in this size range.

Methods

Experimental Section. Experiments were performed on a 2.75 T Fourier transform ion cyclotron resonance mass spectrometer equipped with an external nanoelectrospray ionization source[38] and a temperature-controlled ion cell.[30] Hydrated transition-metal ions were generated by nanoelectrospray ionization from aqueous solutions of ~1 mM metal(II) salts. A positive potential of ~500 V was applied to a platinum wire in direct contact with the aqueous solutions contained in a borosilicate capillary (tip diameter of 1−2 μm) relative to the capillary entrance to the mass spectrometer. Ions were transferred through five stages of differential pumping and accumulated in the ion cell for 3 s, during which time dry $N_2(g)$ was pulsed into the vacuum chamber surrounding the ion cell to a pressure of $\sim 10^{-6}$ Torr to enhance trapping and thermalization of the ions. A mechanical shutter was closed after ion accumulation to prevent additional ions from entering the cell. A delay of 4 s after accumulation ensures that the pressure of the vacuum chamber surrounding the ion cell returns to $< \sim 10^{-8}$ Torr and that the ions have steady-state internal energy distributions. A copper jacket surrounding the ion cell was equilibrated to a temperature of 133 K for at least 8 h prior to data acquisition.

For UV photodissociation experiments, an ensemble of three neighboring cluster ions ($n > 90$), or individual ions ($n < 90$), were isolated using SWIFT techniques. The ensemble method makes it possible to acquire data for large clusters with improved *S/N*.[60] After a delay of 50 ms, a mechanical shutter controlled by a rotary solenoid (Ledex, OH, U.S.A., part number: 810-28-330) was opened, and UV light (193.3 ± 0.5 or 248.4 ± 0.2 nm, corresponding to 6.41 ± 0.02 or 4.991 ± 0.004 eV, respectively; ~8 W) from an excimer laser (EX100, GAM Laser Co., Florida, U.S.A.) was focused through a 1 m focal length CaF_2 lens (~1.25 m from the ion cell center) and entered the vacuum chamber through a CaF_2 window. After the ions were irradiated for 0.5−5 s, the mechanical shutter was closed to prevent laser light from entering the ion cell during detection. The front and back trapping plates of the cylindrical ion cell had radially centered 1.5 in. diameter holes that were slightly modified from the original design[30] such that Cu wire did not span the holes in the trap plates. This ensured that the laser light could pass directly through the ion cell without forming laser ablation products. After a delay of 50 ms, precursor and product ions were detected simultaneously.

Blackbody infrared radiative dissociation kinetics were obtained for $M^{2+}(H_2O)_n$ (M = Co and Cu), for n from 15 to 65, by storing these ions for up to 8 s in the ion cell at 133 K prior to detection. The precursor dissociation was measured for a minimum of four delay times (t). BIRD rate constants, k_{BIRD}, were obtained from linear regression best fits of $\ln([I_n]_t/[I_n]_0)$ versus time, where $[I_n]_t$ is the abundance of $M^{2+}(H_2O)_n$ at the storage time, t, and $[I_n]_0$ is the sum of the abundances for $M^{2+}(H_2O)_n$ and all BIRD products at time t. These kinetic data are first-order for all clusters investigated.

Calculations. The amount of energy deposition required to "boil" off the observed number of water molecules lost in a rapid heating process (such as for UV photodissociation or electron capture dissociation) can be obtained from the average number of water molecules, the sum of the sequential binding energies of the water molecules lost, and the energy that partitions into rotations, translations, and vibrations (E_{RTV}) of the products for each sequential water molecule that is lost.[50,52] In cases where the internal energy deposition is unknown, such as electron capture dissociation experiments,[13,14,49−58] values for the sequential water molecule binding energies are required to determine the amount of internal energy deposited. Because sequential water molecule threshold binding energies to large hydrated divalent metal ion clusters (for $n > 14$) have not been previously measured, these values were obtained from a discrete implementation of the TLDM.[44] When the energy deposited is known, such as in these photodissociation experiments, values for the sequential water molecule binding energies that do not depend on the TLDM, can be accurately determined. E_{RTV} values were obtained by calculating the effective temperature and internal energy of the clusters for each water molecule lost, assuming that all of the energy was instantaneously deposited and full energy randomization occurred prior to water evaporation.

Consider the sequential evaporation of x water molecules from a cluster that starts with n_0 water molecules

$$M^{2+}(H_2O)_{n_0} \xrightarrow{i=1} M^{2+}(H_2O)_{n_0-1} + H_2O \xrightarrow{i+1} \cdots M^{2+}(H_2O)_{n_0-x} + x(H_2O)$$

For instantaneous conversion of electronic-to-vibrational energy, the energy E_D required for this process can be obtained from the following system of equations

$$U_0(T^*_0) = U_P(133\,\mathrm{K}) + E_D \tag{1}$$

$$U_i(T^*_i) = U_{i-1}(T^*_{i-1}) - E_{n,n-1} - \left(\frac{5}{2}\right)kT^*_{i-1} \tag{2}$$

where $U_P(133\ \mathrm{K})$ is the average internal energy of the initial precursor ion-thermalized to a temperature of 133 K. U_i is the average internal energy of the ith cluster, where i is the number of water molecules lost to form this cluster. $E_{n,n-1}$ is the binding energy of the water molecule lost from each cluster, which is obtained from the discrete implementation of the TLDM when the value of E_D is unknown. The energy partitioned into translational and rotational modes of the products for each water molecule lost is given by $(5/2)kT^*_{i-1}$, obtained from the Klots's water cluster evaporation model,[61] where T^*_{i-1} is the effective temperature of the $(i-1)$ cluster and k is the Boltzmann constant. Under these conditions, energy that partitions into the vibrational modes of the water molecules that are lost should be negligible. Average internal energies were obtained from harmonic frequencies calculated for a B3LYP/LACVP**++ energy-minimized structure of $Ca(H_2O)_{14}^{2+}$ and scaled by the vibrational degrees-of-freedom of the cluster of interest.[50,52] E_D is given by

$$E_D = \sum E_{n,n-1} + \left(\frac{5}{2}\right)k \sum T^*_{i-1} \tag{3}$$

where $\sum E_{n,n-1}$ is the sum of the threshold dissociation energy values for each lost water molecule and $(5/2)k \sum T^*_{i-1}$ is the sum of the energy partitioned into the products for each sequential water molecule lost. The system of equations represented by eqs 1−3 has the same number of equations as unknowns (T^* values and E_D) and can be readily solved to obtain values for T^* and E_D.

If the photon energy is completely converted into internal energy of the ion, that is, fluorescence and/or formation of long-lived electronic excited states[46] do not occur, then the average number of water molecules lost can be used to calculate an average threshold binding energy value for all of the water molecules lost ($\langle E_{n,n-1}\rangle$). To calculate $\langle E_{n,n-1}\rangle$, $E_{n,n-1}$ values (previously calculated with the discrete implementation of the TLDM)[44] are substituted with the unknown $\langle E_{n,n-1}\rangle$ value in eqs 1−3, and E_D is substituted with the known photon energy ($h\nu = 6.42$ or 4.99 eV), resulting in a system of equations that can be solved to obtain $\langle E_{n,n-1}\rangle$, the average threshold binding energy for the clusters from n_0 to $n_0 - x$, the average size of which is $n_0 - x/2$. The average sequential water molecule binding enthalpy for each water molecule lost $\langle \Delta H_{n,n-1}\rangle$, is obtained from

$$\Delta H_{n,n-1} = E_{n,n-1} + kT \tag{4}$$

where the vibrational energy lost upon water loss is approximated as being equal to the gained translational, rotational, and vibrational energy of the products ($kT = 0.6$ kcal/mol at 298 K). For large clusters ($n > 90$) where three precursor ions are isolated, a weighted average is used in place of the individual precursor size in the above analysis.[60]

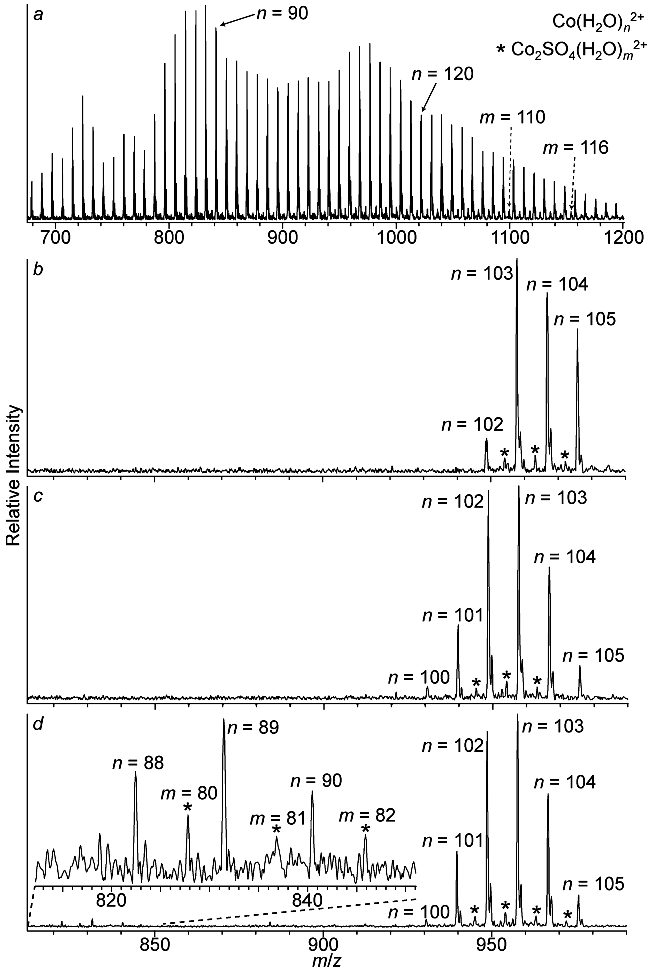

Figure 1. (a) Electrospray ionization mass spectrum of a ∼1 mM aqueous solution of $CoSO_4$ showing distributions of $Co(H_2O)_n^{2+}$ and $Co_2SO_4(H_2O)_m^{2+}$, (b) blackbody infrared radiative dissociation (BIRD) mass spectrum of isolated $Co(H_2O)_{103-105}^{2+}$ at 50 ms, (c) BIRD at 1 s, and (d) 1s 193 nm photodissociation mass spectrum, which is the same as (c) except with 193 nm light entering the ion cell. Inset is a 20× vertical expansion of m/z = 812−851. Asterisks indicate $Co_2SO_4(H_2O)_m^{2+}$ clusters.

Results and Discussion

Ultraviolet Photodissociation of Hydrated Transition-Metal Ions. Broad distributions of $Co^{2+}(H_2O)_n$ (n = 72−139 shown in Figure 1a) and other hydrated divalent ions can be formed by nanoelectrospray ionization and trapped in a cell that is surrounded by a copper jacket at 133 K. A minor distribution of $Co_2SO_4(H_2O)_m^{2+}$ is also observed (m = ~80−122; Figure 1a). BIRD spectra (133 K) of an isolated ensemble of neighboring clusters, $Co^{2+}(H_2O)_{103-105}$ at 50 ms and 1 s, are shown in Figure 1b and c, respectively. At 50 ms, some $Co^{2+}(H_2O)_{102}$ is formed (12.3% relative abundance). At 1 s, the ion distribution shifts to smaller cluster sizes from an average of 103.768 ± 0.005 to 102.737 ± 0.004 water molecules. A photodissociation spectrum of this same isolated $Co^{2+}(H_2O)_{103-105}$ ensemble with 1 s of 193.3 ± 0.5 nm irradiation is shown in Figure 1d. In addition to the distribution resulting from 1 s of BIRD, a relatively narrow distribution of product ions, $Co^{2+}(H_2O)_{88-90}$, formed by absorption of a single 193 nm photon is observed. The average number of water molecules lost from the precursor distribution by absorption of the 193 nm photon, $\langle x \rangle$, is given by the difference in the average precursor cluster size ($\langle n \rangle_f$), 102.737 ± 0.004, and the average product ion distribution ($\langle p \rangle_f$), 88.94 ± 0.06, or 13.80 ± 0.06 water molecules. The average precursor cluster size for the entire irradiation time ($\langle n \rangle$) is obtained from the average of the isolated distribution ($\langle n \rangle_{iso}$), and the distribution after irradiation is complete ($\langle n \rangle_f$), that is, $\langle n \rangle = (103.768 + 102.737)/2 = 103.253 \pm 0.007$.

The energy removed by each water molecule that is lost is given by $h\nu/\langle x \rangle = 6.41$ eV/13.80 = 0.46 eV. This value is an upper limit to the average $E_{n,n-1}$ of each water molecule lost and is slightly higher than the water molecule binding energy that is calculated using a discrete implementation of the TLDM (~0.4 eV).[44] The average energy removed per water molecule should be higher than $E_{n,n-1}$ because some E_{RTV} partitions into the products. Because the energy removed per water molecule lost is only slightly higher than the calculated $E_{n,n-1}$ value, we conclude that the energy of the absorbed 193 nm photon is fully converted into internal energy of the precursor ions, that is, fluorescence and/or formation of long-lived electronic excited states does not occur. These results also indicate that loss of water clusters, which is entropically unfavorable, does not occur to any significant extent.

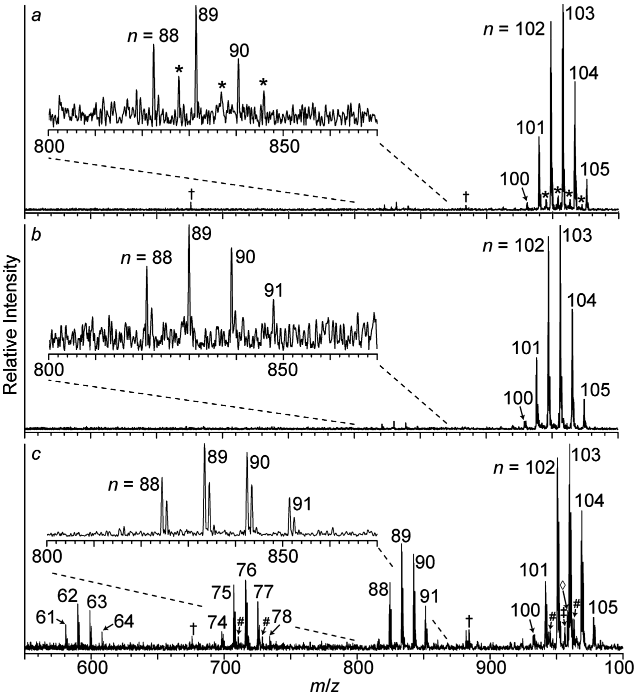

Figure 2. A 1 s ensemble 193 nm photodissociation mass spectra of isolated $M(H_2O)_{103-105}^{2+}$, for M = (a) Co, (b) Fe, and (c) Cu. Peaks corresponding to $M(H_2O)_n^{2+}$ are labeled by n. Symbols indicate $Co_2SO_4(H_2O)_n^{2+}$(∗), electronic noise (†), $CuOH(H_2O)_n^+$ (#), $Cu_2SO_4(H_2O)_{94}^{2+}$ (◊), and $H^+(H_2O)_{53}$ (‡).

Photodissociation mass spectra (193 nm) of $M^{2+}(H_2O)_{103-105}$, M = Co, Fe, and Cu, with 1 s of irradiation, are shown in Figure 2a−c, respectively. Photodissociation of $Fe^{2+}(H_2O)_{103-105}$ results in the formation of $Fe^{2+}(H_2O)_{88-91}$ (Figure 2b), which corresponds to the loss of an average of 13.49 ± 0.08 water molecules from the precursor ions as a result of the absorption of a 193 nm photon and is close to that obtained for Co, $\langle x \rangle$ = 13.80 ± 0.06. The photodissociation efficiencies of Fe and Co are both very low (3.2 and 2.4% photofragment yield, respectively) compared to $Cu^{2+}(H_2O)_{103-105}$, which absorbs 193 nm light more strongly (Figure 2c; ~50.1% photofragment yield). In addition to the formation of $Cu^{2+}(H_2O)_{88-91}$, two additional distributions are formed, $Cu^{2+}(H_2O)_{74-78}$ and $Cu^{2+}(H_2O)_{61-64}$. These distributions correspond to the loss of an average of 13.4, 26.9, and 40.4 water molecules from the precursor distribution as a result of the absorption of 1, 2, and 3 UV photons, respectively. From these data, an average of 13.38 ± 0.02, 13.50 ± 0.03, and 13.49 ± 0.03 water molecules are lost from $Cu^{2+}(H_2O)_{100-105}$, $Cu^{2+}(H_2O)_{88-91}$, and $Cu^{2+}(H_2O)_{74-78}$, respectively. If two photons were absorbed by $Cu^{2+}(H_2O)_{100-105}$ simultaneously or near simultaneously to form $Cu^{2+}(H_2O)_{74-78}$ (or three to form $Cu^{2+}(H_2O)_{61-64}$), then the activated $Cu^{2+}(H_2O)_{100-105}$ should be at a higher effective cluster temperature than that if only one photon was absorbed. More E_{RTV} partitions into the products at higher cluster effective temperatures. If multiple photons are absorbed prior to significant dissociation, the average number of water molecules lost per photon absorbed will be less than that if each photon is absorbed sequentially. Because the number of water molecules lost from each distribution is nearly identical, we conclude that the photons are absorbed by each sequential distribution, and multiphoton absorption by the original precursor is negligible.

Effects of Photon Energy and Cluster Size. The average number of water molecules lost for $M^{2+}(H_2O)_n$ (M = Co, Fe, Cu, Mn, and $CeNO_3$; $\langle n \rangle$ between ~24 and 131) at 248 and 193 nm as a function of the average precursor cluster size is shown in Figure 3. Absorption of a single 6.4 eV photon results in a greater number of water molecules lost ($\langle x \rangle \approx 11-14$ for $\langle n \rangle$ between 24 and 131) than absorption of a single 5.0 eV photon ($\langle x \rangle \approx 8-10$ for $\langle n \rangle$ between 24 and 124) by at least two water molecules for $\langle n \rangle$ greater than ~30. The extent of water loss also depends significantly on the precursor cluster size. For example, an average of 8.57 and 10.69 water molecules is lost from $Fe(H_2O)_{24}^{2+}$ and $Fe(H_2O)_{\sim 124}^{2+}$, respectively, when a single 248 nm photon is absorbed. Fewer water molecules are lost at the smaller cluster sizes because water molecule binding energies and E_{RTV} values increase with decreasing cluster size. For larger clusters, these effects depend less strongly on size, and thus, the average number of water molecules lost also depends less on size. There is no evidence of ion fluorescence or formation of long-lived electronic excited states at any cluster size at either excitation wavelength.

Irradiation Time and Kinetic Shift Effects. Because of the low-photon absorption efficiency for most of the ions (with the exception of $Cu^{2+}(H_2O)_n$ at 193 nm), relatively long irradiation times are required to observe photodissociation products under these conditions. During laser irradiation, both the precursors and the photofragment products will undergo dissociation as a result of BIRD. To the extent that the product and precursor ion distributions dissociate at the same rate, $\langle x \rangle$ will reflect the average number of water molecules lost due to photon absorption alone. This should be increasingly true for shorter irradiation

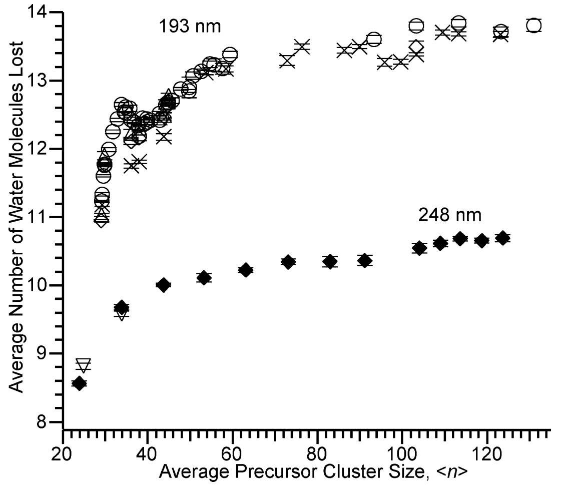

Figure 3. Average number of water molecules lost as a result of absorption of a 193 nm (6.4 eV) photon by $M(H_2O)_n^{2+}$, M = Co (○), Mn (Δ), Fe (◇), and Cu (×), and absorption of a 248 nm (5.0 eV) photon by $M(H_2O)_n^{2+}$, M = Fe(♦) and $CeNO_3$ (∇), as a function of the average ensemble precursor cluster size. UV irradiation times vary from 0.5 to 5 s. Error bars indicate the propagated uncertainty from the noise in each mass spectrum.

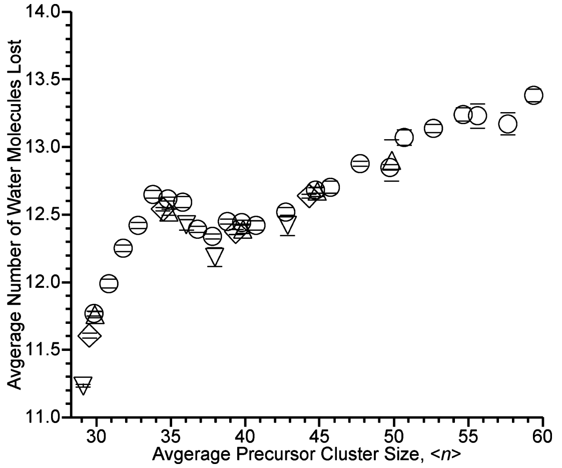

Figure 4. Average number of water molecules lost from hydrated Co^{2+} clusters upon absorption of a 193 nm photon as a function of the average precursor cluster size (⟨*n*⟩) using an irradiation time of 0.5 (Δ), 1 (○), 3 (◇), and 5 (∇) s.

times and for larger clusters for which the BIRD rate constants do not depend strongly on size over a relatively small range in cluster sizes. To investigate the effects of BIRD on the average number of water molecules lost, 193 nm photodissociation data for $Co(H_2O)_n^{2+}$ was acquired using irradiation times of 0.5, 1, 3, and 5 s (Figure 4). The average number of water molecules lost does not depend significantly on irradiation time (within 0.1 water molecules), indicating that the BIRD rates of the precursor and UV photofragments are sufficiently similar that this BIRD correction method is adequate.

For a fixed amount of internal energy deposited, the time required for water molecule evaporation to occur will increase with increasing cluster size, owing to the greater number of degrees of freedom. If dissociation is slow relative to the experimental time scale, there will be a kinetic shift. To test for a kinetic shift in these experiments, $Fe^{2+}(H_2O)_{124-126}$ was irradiated for 1 s with 248 nm light, and ions were detected after a delay of 50 ms to 1 s. An average number of 10.7, 10.6, 10.8, and 10.5 water molecules were lost (BIRD corrected) with a delay of 50, 250, 500, and 1000 ms, respectively. Irradiation of $Co^{2+}(H_2O)_{133-135}$ results in an average of 13.8 and 13.7 water molecules lost at 50 ms and 0.5 s, respectively. These results indicate that any effects of a kinetic shift for clusters with $n \leq \sim 135$ are negligible for delay times of 50 ms or longer, and in this work, a delay of 50 ms between the end of ion irradiation and ion detection is used for all other photodissociation experiments.

Metal Ion Identity. Although the metal ion can significantly affect the UV absorption cross sections (Figure 2), there is a much smaller effect of metal ion identity on the extent of water molecule loss for a given cluster size. For example, upon 193 nm photon absorption by $M^{2+}(H_2O)_{36}$, M = Co, Fe, Mn, and Cu, an average of 12.43, 12.23, 12.10, and 11.75 water molecules is lost, respectively (Figure 3). For M = Cu and Co, this corresponds to a difference of (6.41 eV/11.75) − (6.41 eV/12.43) = 0.03 eV per water molecule lost, that is, each water molecule lost from $Cu^{2+}(H_2O)_{36}$ removes an average of 0.03 eV more energy than that from $Co^{2+}(H_2O)_{36}$.

To investigate why a slightly different number of water molecules is lost from Co compared to Cu, BIRD rate constants, which are very sensitive to $E_{n,n-1}$ values, were measured (Figure 5). The extent of BIRD depends on $E_{n,n-1}$, the infrared radiative absorption and emission rates of the cluster, and the number of water molecules at the surface of the cluster that can be lost (degeneracy factor). The kinetic data at 133 K for $M^{2+}(H_2O)_{35}$ and $M^{2+}(H_2O)_{16}$ (M = Co and Cu) are shown in Figure 5a. The larger cluster dissociates more rapidly than the smaller cluster predominantly because of greater radiative absorption rates, although slightly decreasing binding energies with increasing cluster sizes may also contribute to this effect. If for a given cluster size the radiative absorption and emission rates and degeneracy factors are similar for different metal ions, then any differences in the BIRD rates should largely be due to differences in $E_{n,n-1}$ values. The measured k_{BIRD} values for $M^{2+}(H_2O)_{16}$ are 0.112 ± 0.005 and 0.123 ± 0.003 s^{-1} for Cu and Co, respectively, suggesting that the binding energy of water to $Cu^{2+}(H_2O)_{16}$ may be slightly higher than that for $Co^{2+}(H_2O)_{16}$, but this difference is negligible for $M^{2+}(H_2O)_{36}$. A linear regression analysis of the dehydration rate constants as a function of cluster size (Figure 5b) results in slopes of 0.018 ± 0.001 and 0.016 ± 0.001 s^{-1} for Cu and Co, respectively. To investigate the effect of binding energies when many water molecules are lost, such as when a 193 nm photon is absorbed, each sequential dehydration rate constant from *n* to *n* − 12 was summed, and these values as a function of *n* are shown in Figure 5c. These summed values for Cu are greater than that of Co (by an average of 0.30 s^{-1} for *n* = 26−42). These results suggest that, on average, $Cu^{2+}(H_2O)_n$ may have slightly lower water molecule binding energies over this range of cluster sizes (*n* = 15−65). However, in the UV photodissociation experiments, the Cu-containing clusters lose slightly fewer water molecules than the Co-containing clusters for $n < \sim 44$, which indicates that the Cu-containing clusters have slightly higher $E_{n,n-1}$ values on average.

This apparent discrepancy, which is very subtle, can be explained by two effects; (1) the Cu- containing clusters have higher infrared absorption cross sections, as is the case at 193 nm, or a slightly higher degeneracy factor, which would lead to larger BIRD rate constants. (2) Alternatively, upon absorption of a UV photon, slightly less energy (<1 kcal/mol) could partition into the translations and rotations of the products for the Co-containing clusters if the water molecules are lost from clusters with lower effective temperatures, which could occur if internal conversion of electronic-to-vibrational energy is slow

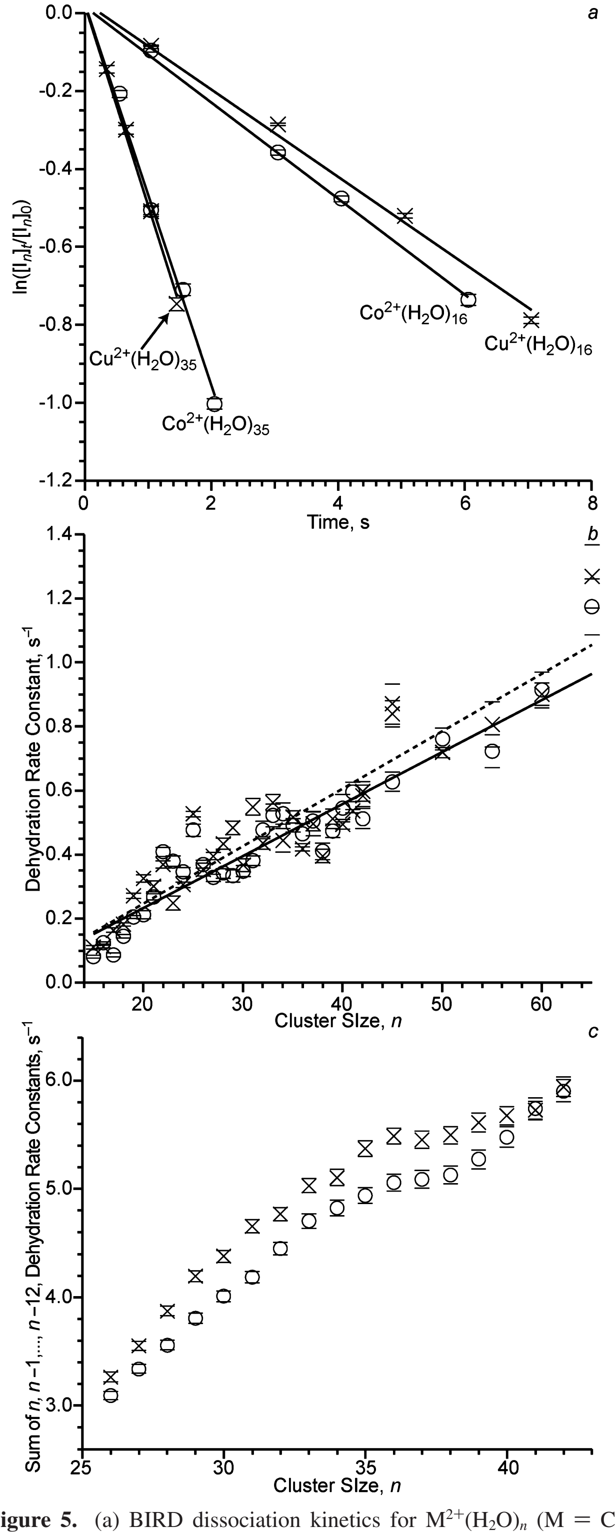

Figure 5. (a) BIRD dissociation kinetics for $M^{2+}(H_2O)_n$ (M = Co (○) and Cu (×), $n = 16$ and 35), (b) dehydration rate constants as a function n, and (c) the sum of the dehydration rate constants from n to $n - 12$ as a function of n.

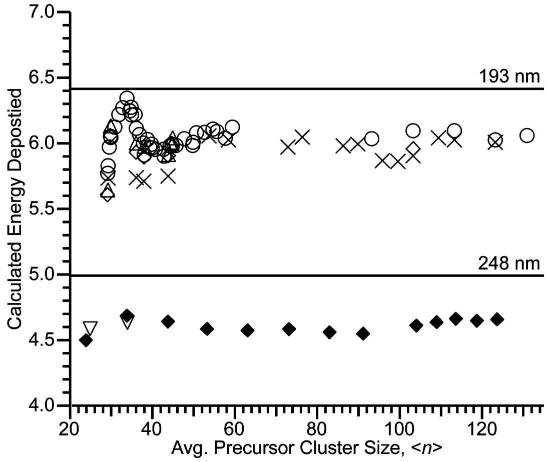

Figure 6. Calculated energy deposited (in eV) obtained from the average number of water molecules lost upon absorption of a 193 or 238 nm photon by $M^{2+}(H_2O)_n$ (markers the same as those in Figure 3), the binding energies of the water molecules lost (calculated using the TLDM), and the energy partitioning model (see Calculations section) as a function of the average precursor clusters size.

compared to the loss of the first water molecule. The effect of metal ion identity on the number of water molecules lost is very subtle at small cluster sizes and becomes negligible at larger cluster sizes ($n > \sim 44$). These results are consistent with electron capture experiments with hydrated divalent and trivalent metal ions which indicate that for smaller clusters with large recombination energies, the rate of ion dissociation, at least for some of the initial water molecules lost, can be competitive with the rate of conversion from electronic-to-vibrational energy, that is, nonergodic dissociation, whereas for larger clusters, the rate of energy conversion occurs much faster than the rate of water molecule loss.[52,55]

The sum of the dehydration rate constants from n to $n - 12$ increases nearly monotonically as a function of cluster size from $n = 26$ to 35, slightly plateaus from $n = 35$ to 37, and continues to increase with increasing size for $n > 37$. The deviation in the monotonically increasing values is similar to the data in Figure 3 for Co, in which the average water molecules lost increases sharply and nearly monotonically from 11.2 to 12.6 for $n = 29-33$, decreases slightly to 12.3 at $n = 37$, and monotonically increases again with increasing size. The slight change in the average binding energies that results in this "bump" feature in both the BIRD and photodissociation data could arise from a structural transition, such as the onset of a third solvent shell or a transition to a larger ion coordination number with increasing cluster size.

Fe was the only hydrated divalent metal ion of the 3d transition-metal ions (of M = Mn−Zn) that absorbed 248 nm photons strongly enough to observe photodissociation under these conditions. To investigate effects of metal ion identity at 248 nm, the average number of water molecules lost upon absorption at 248 nm by $CeNO_3^{2+}(H_2O)_n$ ($n = 32$ and 25) was investigated. The Fe^{2+}- and $CeNO_3^{2+}$-containing water clusters both lose essentially the same number of water molecules at a given cluster size (Figure 3), indicating that the ion identity has only a subtle effect.

Evaluation of Energy Deposition Model. The energy deposited into a hydrated ion can be determined from the average number of water molecules lost, the sum of the threshold binding energies, and the sum of the E_{RTV} values for each sequential water molecule lost.[50,52] The TLDM[44] is used to calculate threshold binding energies to larger clusters for which experimental data is not available, and a statistical model[61] is used to determine the energy partitioning. To evaluate the accuracy with which the energy deposited upon ion activation can be obtained from these models, the energy deposited into the clusters is calculated from the number of water molecules lost and is compared to the known photon energies in Figure 6. In general, the energy deposition values obtained by modeling the experimental data are nearly constant over a wide range of cluster sizes (for $n > 40$) for both photon energies (Figure 6),

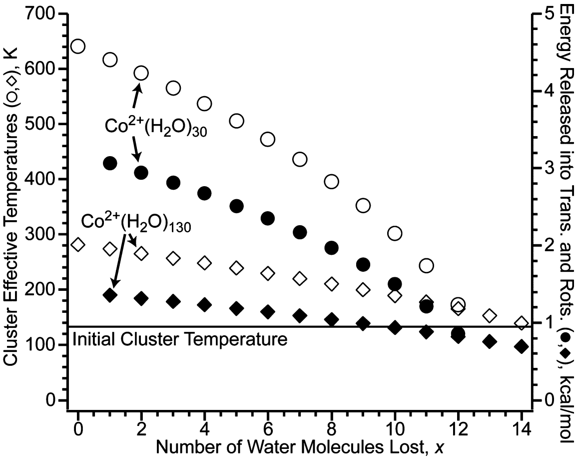

Figure 7. Calculated cluster effective temperatures (open symbols, left axis) and energy released into the translations (Trans.) and rotations (Rots.) of the products (closed symbols, right axis) upon absorption of a 193 nm photon by $Co^{2+}(H_2O)_{30}$ and $Co^{2+}(H_2O)_{130}$ as a function of the number of water molecules lost. Horizontal line indicates the initial temperature of the precursor clusters.

whereas the average number of water molecules lost increases substantially over this same size range (Figure 3). The values obtained by modeling the measured water molecule loss are, on average, 0.41 ± 0.13 eV and 0.38 ± 0.05 eV lower than the energy of the absorbed photons (6.4 and 5.0 eV, respectively). Thus, the values obtained using the TLDM and energy partitioning model underestimate the actual energy deposited by 6.5 and 7.7% for absorption of a 6.4 and 5.0 eV photon, respectively. The deviation between the calculated values and actual energy deposited for each photon energy is small, and the calculated values are nearly constant over a wide range of cluster sizes. Because the E_{RTV} values depend strongly on cluster size and photon energy, these data indicate that the dominant source of the systematic error in the combined models is likely a direct result of the calculated threshold binding energy values obtained from the TLDM being lower than the actual values.

Effective Temperatures and Kinetic Energy Release. The effective temperature of the cluster depends upon the initial energy deposited into the ion, the cluster size, and the number of water molecules lost. For example, the calculated cluster effective temperatures of $Co^{2+}(H_2O)_{30}$ and $Co^{2+}(H_2O)_{130}$ increase to 640 and 280 K (from an initial temperature of 133 K), respectively, upon absorption of a 193 nm photon (Figure 7). Sequential water molecule loss reduces the cluster effective temperature to near the initial ion temperature. Because the energy deposition is the same (6.4 eV), the larger ion is heated to a lower temperature because the deposited energy is spread over many more degrees of freedom. The average energy that partitions into the products for each sequential water molecule lost, $(^5/_2)kT^*$, is plotted on the right axis as a function of the number of water molecules lost. More energy partitions into translations and rotations for the smaller cluster because the water molecules are lost from clusters with higher effective temperatures.

Average Binding Enthalpies from UV Photodissociation Data and the E_{RTV} Model. The average ensemble sequential water molecule binding enthalpies to $M^{2+}(H_2O)_n$ ($\langle\Delta H_{n,n-1}\rangle$), obtained from the UV photodissociation data and E_{RTV} model, as a function of the average cluster size for each water molecule that is lost ($\langle n\rangle - \langle x\rangle/2 = \sim19-124$) are shown in Figure 8. The average ensemble water molecule binding enthalpies decrease from 11.6 kcal/mol for an average cluster size of ~19 to an average value of 10.3 ± 0.1 kcal/mol that is essentially constant for clusters with more than ~40 water molecules. The binding enthalpies level off to a value that is just slightly lower than the bulk heat of vaporization (10.5 kcal/mol at 298 K) at large sizes,[45,62,63] indicating that water−water interactions, as opposed to ion−water interactions, dominate the binding energy of the surface water molecules in the larger clusters.

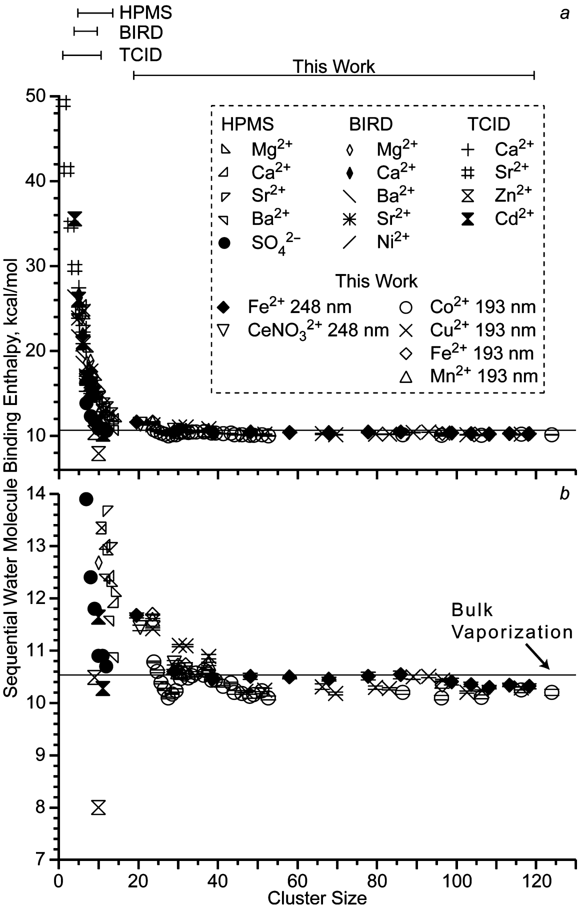

Figure 8. Average ensemble sequential binding enthalpies ($\langle\Delta H_{n,n-1}\rangle$) measured for $M^{2+}(H_2O)_n$ (M = Co, Fe, Mn, Cu, and $CeNO_3$; $\langle n\rangle - \langle x\rangle/2 = \sim18-125$) obtained from UV photodissociation experiments at 193 and 248 nm (see legend) as a function the average cluster size ($\langle n\rangle - \langle x\rangle/2$), compared to sequential binding enthalpies from high-pressure mass spectrometry (HPMS),[27,36] blackbody infrared radiative dissociation (BIRD),[28−30] and threshold collision-induced dissociation (TCID)[31−34] as a function of n. Data is shown for enthalpy values from (a) 7 to 50 kcal/mol and (b) 7 to 14 kcal/mol. The size range of previous measurements (HPMS, BIRD, and TCID) and that of the current work are indicated in the inset of (a). The horizontal line indicates the bulk heat of vaporization at 298 K.

For comparison, sequential water molecule binding enthalpy values ($\Delta H_{n,n-1}$) to divalent ions measured using HPMS,[27,36] BIRD,[28−30] and TCID[31−34] as a function of n are included (for n up to 14 in Figure 8). The values obtained from the UV photodissociation measurements (average clusters sizes from ~19 to 124) are in excellent agreement with the trend in values from HPMS, BIRD, and TCID for $M^{2+}(H_2O)_n$ (n up to 14). The average ensemble enthalpy values obtained from either 248 or 193 nm agree with each other to within 0.5 kcal/mol. We estimate the absolute uncertainty in our sequential average ensemble binding enthalpy values to be ±1 kcal/mol,[64] which is comparable to the uncertainty reported for the other thermochemical methods[27−34] for obtaining sequential binding enthalpies at smaller cluster sizes. This method has the advantage that these measurements can be readily made on very large clusters (well past three solvent shells) and complements the traditional thermochemical methods[27−34] that have been used to measure the binding enthalpies of water molecules in the first and second hydration shells (see inset, Figure 8a).

The values obtained for the divalent ions here are in good agreement with, but slightly higher than, those reported by Castleman and co-workers[25] for $H^+(H_2O)_n$ (n up to 28). For example, the average water molecule binding energy values to $Fe^{2+}(H_2O)_n$ obtained from the UV photodissociation experiments for average cluster sizes of ∼19.6 and 29.0 water molecules are 11.1 and 10.0 kcal/mol, respectively, whereas for $H^+(H_2O)_n$, the binding energy values obtained from metastable decay experiments[25] are 10.8 and 9.3 kcal/mol for the $n = 20$ and 28 clusters, respectively. However, the sequential water molecule binding energy values for $H^+(H_2O)_n$ obtained from collision-induced dissociation experiments[26] in a triple-quadrupole mass spectrometer are significantly lower ($E_{n,n-1}$ values of 7.0 and 8.2 kcal/mol for $n = 20$ and 28, respectively) than the values obtained from either the UV photodissociation or from the metastable decay measurements. At these relatively large cluster sizes, the metal ion charge state should have only a minimal effect on the water molecule binding energies.

The ions in the FT/ICR cell may have a temperature that is somewhat higher than that of the surrounding copper jacket, owing to absorption of photons originating from outside of the copper jacket and from heat transfer along electrical connections to the cell plates. The average sequential water molecule binding enthalpy determined from the 193 nm photodissociation data for $Co(H_2O)_{26}{}^{2+}$ assuming an initial ion temperature of 133 or 191 K is 10.8 or 10.6 kcal/mol, respectively. For an average cluster size of ∼124 water molecules, values for the average sequential water molecule binding enthalpy of 10.2 and 10.0 kcal/mol are obtained for 133 and 191 K, respectively. Thus, the actual initial ion temperature only slightly affects the values obtained for the average sequential water molecule binding enthalpies from this method and should not be a significant source of uncertainty.

Cluster Temperature Effects Upon Photon Absorption. The effective temperatures of the clusters after absorption of a UV photon depend strongly on the cluster size and can be quite high prior to water loss (Figure 7). The average effective temperatures of the clusters during the evaporation process, calculated by averaging the cluster temperature for each water molecule lost, is plotted as a function of the average cluster size ($\langle n\rangle$ - $\langle x\rangle/2$) in Figure 9a. For example, when $Co^{2+}(H_2O)_{30}$ absorbs a 193 nm photon, its effective temperature prior to any water loss is 640 K, but the average effective temperature is ∼440 K for all water molecules lost (Figures 9a and 7). For cluster sizes from ∼40 to 125 water molecules, the average sequential binding enthalpies are essentially constant (10.3 ± 0.1 kcal/mol), whereas the average effective temperatures of each cluster formed as a result of water molecule loss upon photon absorption decrease from ∼360 to 230 K and ∼330 to 220 K for 193 and 248 nm photon absorption, respectively (Figure 9).

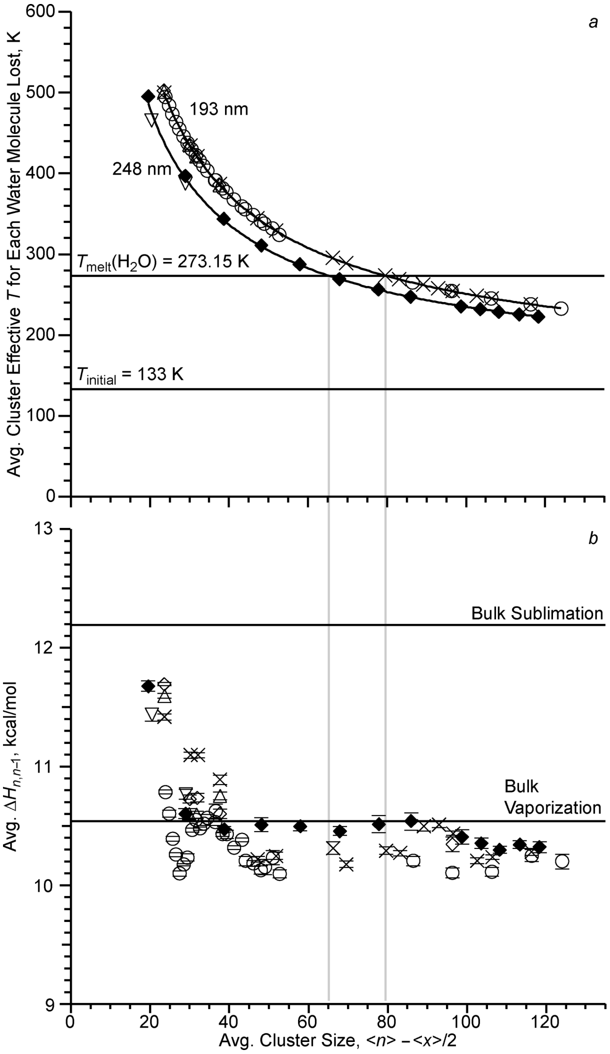

Figure 9. (a) Average of the calculated effective temperatures of each cluster formed upon sequential water molecule loss at 193 and 248 nm and (b) average ensemble sequential binding enthalpies ($\langle\Delta H_{n,n-1}\rangle$) measured for $M^{2+}(H_2O)_n$ (M = Co, Fe, Mn, Cu, and $CeNO_3$; $\langle n\rangle - \langle x\rangle/2$ = ∼18−125) obtained from UV photodissociation experiments at 193 and 248 nm (same ion markers as those in Figure 3) as a function the average cluster size ($\langle n\rangle - \langle x\rangle/2$). The labeled horizontal lines indicate the melting point of bulk water ($T_{melt}(H_2O)$), the initial cluster temperature ($T_{initial}$), the 298 K bulk heat of vaporization (Bulk Vaporization), and the 273 K bulk heat of sublimation (Bulk Sublimation). Vertical gray lines indicate the cluster size at which the average cluster effective temperature is equal to the melting point of bulk water. Effective temperatures are fit with power functions as a guide.

Although the initial cluster temperature (133 K) is substantially lower than the melting point of pure hexagonal ice (273 K), the $\Delta H_{n,n-1}$ values obtained from these experiments are closer to the heat of water vaporization (10.5−10.7 kcal/mol for $T = 293-273$ K)[45] than the bulk heat of ice sublimation (12.2 kcal/mol),[63] which is significantly larger. Moreover, there does not appear to be a significant trend in the $\Delta H_{n,n-1}$ values with cluster size or photon energy even though both factors significantly affect the average cluster effective temperatures at which water molecules are lost (Figure 9a). These clusters may be more like bulk liquid water as a result of melting point depression, such as that recently reported for $(H_2O)_n{}^-$, for n = 48 and 118, in which a melting transition for these clusters was reported at temperatures of 93 and 118 K, respectively.[42] Ion impurities in water clusters can pattern water at relatively long distances,[65] which disrupts the water network relative to a pure water cluster. Because these clusters are formed by solvent evaporation from electrospray droplets,[38,66] rapid evaporative cooling may kinetically trap these clusters into structures that are more like bulk liquid water than ice. These data also indicate that the cluster structures do not significantly change when rapidly heated for a short amount of time, that is, sequential water molecule loss rapidly cools the cluster after photon absorption and before any large-scale structural rearrangements

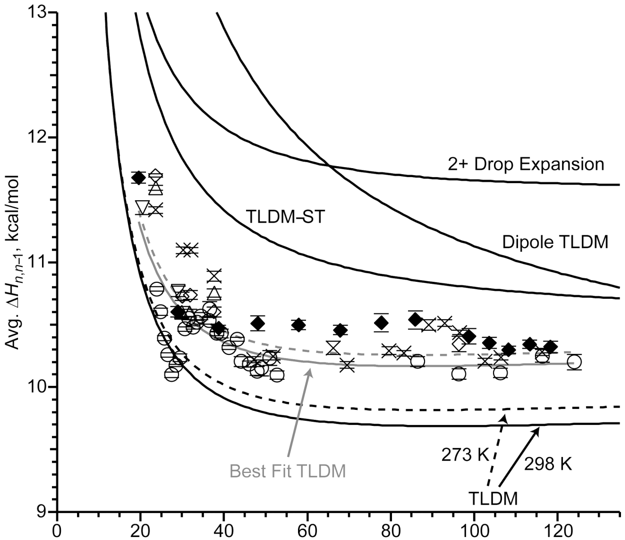

Figure 10. Average ensemble sequential binding enthalpies measured for $M^{2+}(H_2O)_n$ (M = Co, Fe, Mn, Cu, and $CeNO_3$; $\langle n\rangle - \langle x\rangle/2 = \sim 19-124$) obtained from UV photodissociation experiments at 193 and 248 nm (same ion markers as those in Figure 3) as a function the average cluster size ($\langle n\rangle - \langle x\rangle/2$). Values for sequential water molecule binding enthalpies to $M(H_2O)_n^{2+}$, calculated using the discrete implementation of the TLDM,[44] the TLDM without surface tension (TLDM−ST), the TLDM modified to include an additional ion−dipole term (Dipole TLDM)[68] parametrized to 298 K, the TLDM parametrized to 273 K (TLDM 273 K),[44] and the liquid drop expansion model (Drop Expansion),[48] are plotted as a function of *n*. Error bars represent uncertainty in the average number of water molecules lost propagated from the noise in the corresponding mass spectra.

or phase transitions that are significant enough to alter the measured water binding enthalpies occur.

Comparison of Liquid Drop Models to Experimental Data. Various implementations of the TLDM have been used to calculate the binding enthalpies (and energies) to large ionic water clusters for a variety of applications.[44,48,59,67,68] Sequential water molecule binding enthalpies obtained from the TLDM include a cluster charging term, a surface tension term, and a bulk binding enthalpy term. $\Delta H_{n,n-1}$ values calculated using the TLDM[44] are plotted in Figure 10 as a function of *n* (solid line labeled TLDM). The charging term, which increases $\Delta H_{n,n-1}$ versus the bulk value, is a result of the difference in enthalpy of charging two dielectric spheres that are about the size of the *n* and $n - 1$ clusters, where the cluster sizes are obtained from the density of bulk water. The surface enthalpy term decreases the binding enthalpy value as a result of the slightly lower surface energy of the $n - 1$ cluster, and omitting this term results in higher values (TLDM-ST; Figure 10). The temperature slightly affects the values obtained from the TLDM; using values for bulk water at 298 versus 273 K increases $\Delta H_{n,n-1}$ by ~0.1 kcal/mol at larger cluster sizes.

Other modified TLDMs have been reported.[48,68] Yu introduced a new ion−dipole term to the TLDM, which included the energy of the ion−dipole interaction between the cluster and the water molecule (Dipole TLDM).[68] Values obtained with this model are significantly higher because this model includes additional energy that is already accounted for by the TLDM.[44] More recently, the Thomson equation has been used to calculate binding energies of protonated water clusters (1+ drop expansion model in Table 1).[48] In this implementation of the model (called drop expansion), sequential water molecule $E_{n,n-1}$ values are approximated as being equal to $\Delta G_{n,n-1}$ values that are calculated using the continuous TLDM[59] with parameters for bulk water at 273 K and a bulk binding energy value of 0.49 eV (*y*-axis offset value). Sequential water binding enthalpy values obtained for divalent ions from the drop expansion model are nearly 2 kcal/mol higher than the values obtained from the TLDM because the value used for the bulk binding energy term (11.9 kcal/mol) is too large (Figure 10).

Although the binding energy values calculated using the TLDM parametrized using bulk values at either 298 or 273 K agree with the experimental data better than the values calculated using the other models, these values are still ~0.5 kcal/mol lower than the experimental values at the larger cluster sizes (Figure 10; Table 1). Values obtained using the TLDM−ST are in better agreement with the experimentally measured values than those from the other models that overestimate binding enthalpy values but are higher than the experimental data by an average of 0.9 kcal/mol. Best fits of the *y*-axis offset value for the TLDM (both temperatures, Figure 10) and the TLDM−ST (data not shown) result in a better fit for the TLDM (ΔAD = 0.2, for 298 and 273 K parameters) than those for the TLDM−ST (ΔAD = 0.3). These data indicate that the TLDM fits the shape of experimental data better than the TLDM−ST.

The TLDM fits the relative size-dependent trend in the data well but is systematically too low. To determine the best effective binding enthalpy term to be used in the TLDM (i.e., the *y*-axis offset) for clusters in this size range, the deviation between the values obtained from the TLDM and the experimental values were minimized, resulting in an effective enthalpy

TABLE 1: Average Absolute Deviation (ΔAD) between Values Calculated with Various Liquid Drop Models and the Experimental Values Obtained from UV Photodissociation Experiments and Best Fit of the *y*-Axis Offset for TLDM and TLDM-ST to Experimental Data[a]

model	ΔAD (kcal/mol)	$\Delta H_{n,n-1}$ (kcal/mol)[h]
TLDM[b]	0.5(2)	$354.44[(n-1)^{-1/3} - n^{-1/3}] + 7.68[(n-1)^{2/3} - n^{2/3}] + 10.54$
TLDM 273 K[c]	0.5(3)	$344.03[(n-1)^{-1/3} - n^{-1/3}] + 8.04[(n-1)^{2/3} - n^{2/3}] + 10.69$
TLDM−ST[d]	0.9(4)	$354.44[(n-1)^{-1/3} - n^{-1/3}] + 10.54$
Dip. TLDM[e]	2.4(1.1)	$\approx 204.62n^{-1.25} + 10.33$[i]
1+ Drop Exp.[f]	0.7(3)	$-3.38n^{-1/3} + 28.83n^{-4/3} + 11.89$
2+ Drop Exp.[g]	1.3(3)	$-3.38n^{-1/3} +115.30n^{-4/3} + 11.89$
TLDM fit	0.2(2)	$354.44[(n-1)^{-1/3} - n^{-1/3}] + 7.68[(n-1)^{2/3} - n^{2/3}] + 11.08$
TLDM 273 K fit	0.2(2)	$344.03[(n-1)^{-1/3} - n^{-1/3}] + 8.04[(n-1)^{2/3} - n^{2/3}] + 11.17$
TLDM-ST fit	0.3(2)	$354.44[(n-1)^{-1/3} - n^{-1/3}] + 9.64$

[a] All models are for hydrated divalent ions, unless indicated otherwise. [b] Discrete implementation of the TLDM parametrized with properties from bulk water at 298 K.[44] [c] TLDM using bulk water parameters at 273.16 K. [d] Discrete implementation of the TLDM (298 K parameters) without the surface tension term. [e] Discrete implementation of the TLDM with the ion−dipole term included (298 K parameters).[68] [f] Liquid droplet model expansion (Drop Exp.) equation for a monovalent cluster.[48] [g] Drop Exp. for a divalent cluster.[48] [h] Can convert to binding energy values using eq 4. [i] Equation approximated from a power fit to enthalpy values calculated using Dip. TLDM.

value of 11.17 kcal/mol using parameters for liquid water at 273 K. This effective enthalpy for clusters this size may account for other uncertainties in the model, or it may indicate that the clusters have some partial ice-like structures.

Conclusions

Water binding enthalpies to clusters containing divalent metal ions and up to 124 water molecules were measured by dissociating trapped thermal ions with UV radiation at 248 and 193 nm. These measurements complement more conventional thermochemical methods that have been used to measure water molecule binding energies to smaller clusters, and these UV photodissocation measurements can be made with comparable accuracy. The binding energies decrease with increasing cluster size for the smaller clusters, but there is a discontinuity of ~34 water molecules for Co^{2+}, which is reproduced by the summed BIRD kinetic data for these clusters, which may be due to a structural transition between a second and third hydration shell when many water molecules are lost. The average binding enthalpies for all ions reach a nearly constant value of ~10.4 kcal/mol for clusters with more than 40 water molecules, a value that is within 1% of the bulk heat of vaporization of water. No evidence for phase transitions, fluorescence, or long-lived excited states was observed. These results indicate that the structure of water in these clusters may be more like that of bulk liquid water than ice, a result that could be due to freezing point depression or kinetic trapping owing to fast evaporative cooling of the initial droplets.

These experimental data follow the trends indicated by the TLDM using parameters for liquid water near 0 °C, but modeled values are lower than the experimental values by an average of ~0.5 kcal/mol. Other models show even larger deviations from the experimental data. These data were fit with a semiempirical equation, which makes it possible to obtain sequential binding enthalpies to large clusters with higher accuracy. This UV photodissociation method can be used to calibrate ion nanocalorimetry data, such as recombination energies of electrons with extensively hydrated ions, which should make it possible to obtain highly accurate thermochemical values, including absolute solution-phase reduction potentials, entirely from experimental data with no modeling.

Acknowledgment. Acknowledgment is made to the donors of the American Chemical Society Petroleum Research Fund (47916-AC6) for support of this research. The authors thank the National Science Foundation (CHE-0718790 and CHE-1012833) for generous financial support. B.N. and D.M.N. acknowledge support from the Director, Office of Basic Energy Sciences, Chemical Sciences Division of the U.S. Department of Energy under Contract No. DE-AC02-05CH11231.

References and Notes

(1) Cramer, C. J.; Truhlar, D. G. *Chem. Rev.* **1999**, *99*, 2161.
(2) Tomasi, J.; Persico, M. *Chem. Rev.* **1994**, *94*, 2027.
(3) Beyer, M. *Mass Spectrom. Rev.* **2007**, *26*, 517.
(4) Meot-Ner, M. *Chem. Rev.* **2005**, *105*, 213.
(5) Castleman, A. W.; Bowen, K. H. *J. Phys. Chem.* **1996**, *100*, 12911.
(6) Coe, J. V.; Lee, G. H.; Eaton, J. G.; Arnold, S. T.; Sarkas, H. W.; Bowen, K. H.; Ludewigt, C.; Haberland, H.; Worsnop, D. R. *J. Chem. Phys.* **1990**, *92*, 3980.
(7) Bragg, A. E.; Verlet, J. R. R.; Kammrath, A.; Cheshnovsky, O.; Neumark, D. M. *Science* **2004**, *306*, 669.
(8) Bragg, A. E.; Verlet, J. R. R.; Kammrath, A.; Cheshnovsky, O.; Neumark, D. M. *J. Am. Chem. Soc.* **2005**, *127*, 15283.
(9) Verlet, J. R. R.; Bragg, A. E.; Kammrath, A.; Cheshnovsky, O.; Neumark, D. M. *Science* **2005**, *310*, 1769b.
(10) Verlet, J. R. R.; Bragg, A. E.; Kammrath, A.; Cheshnovsky, O.; Neumark, D. M. *Science* **2005**, *307*, 93.
(11) Kammrath, A.; Verlet, J. R. R.; Griffin, G. B.; Neumark, D. M. *J. Chem. Phys.* **2006**, *125*, 076101.
(12) Asmis, K. R.; Santambrogio, G.; Zhou, J.; Garand, E.; Headrick, J.; Goebbert, D.; Johnson, M. A.; Neumark, D. M. *J. Chem. Phys.* **2007**, *126*, 191105.
(13) Donald, W. A.; Leib, R. D.; O'Brien, J. T.; Holm, A. I. S.; Williams, E. R. *Proc. Natl. Acad. Sci. U.S.A.* **2008**, *105*, 18102.
(14) Donald, W. A.; Demireva, M.; Leib, R. D.; Aiken, M. J.; Williams, E. R. *J. Am. Chem. Soc.* **2010**, *132*, 4633.
(15) Bush, M. F.; Saykally, R. J.; Williams, E. R. *Chem. Phys. Chem.* **2007**, *8*, 2245.
(16) Bush, M. F.; Saykally, R. J.; Williams, E. R. *J. Am. Chem. Soc.* **2008**, *130*, 15482.
(17) Bush, M. F.; Saykally, R. J.; Williams, E. R. *J. Am. Chem. Soc.* **2008**, *130*, 9122.
(18) Garand, E.; Wende, T.; Goebbert, D. J.; Bergmann, R.; Meijer, G.; Neumark, D. M.; Asmis, K. R. *J. Am. Chem. Soc.* **2010**, *132*, 849.
(19) Goebbert, D. J.; Garand, E.; Wende, T.; Bergmann, R.; Meijer, G.; Asmis, K. R.; Neumark, D. M. *J. Phys. Chem. A* **2009**, *113*, 7584.
(20) Kebarle, P.; Searles, S. K.; Zolla, A.; Scarborough, J.; Arshadi, M. *J. Am. Chem. Soc.* **1967**, *89*, 6393.
(21) Džidić, I.; Kebarle, P. *J. Phys. Chem.* **1970**, *74*, 1466.
(22) Searles, S. K.; Kebarle, P. *Can. J. Chem.* **1969**, *47*, 2619.
(23) Rodgers, M. T.; Armentrout, P. B. *J. Phys. Chem. A* **1997**, *101*, 1238.
(24) Kebarle, P. *Annu. Rev. Phys. Chem.* **1977**, *28*, 445.
(25) Shi, Z.; Ford, J. V.; Wei, S.; Castleman, A. W. *J. Chem. Phys.* **1993**, *99*, 8009.
(26) Magnera, T. F.; David, D. E.; Michl, J. *Chem. Phys. Lett.* **1991**, *182*, 363.
(27) Peschke, M.; Blades, A. T.; Kebarle, P. *J. Phys. Chem. A* **1998**, *102*, 9978.
(28) Rodriguez-Cruz, S. E.; Jockusch, R. A.; Williams, E. R. *J. Am. Chem. Soc.* **1998**, *120*, 5842.
(29) Rodriguez-Cruz, S. E.; Jockusch, R. A.; Williams, E. R. *J. Am. Chem. Soc.* **1999**, *121*, 8898.
(30) Wong, R. L.; Paech, K.; Williams, E. R. *Int. J. Mass Spectrom.* **2004**, *232*, 59.
(31) Carl, D. R.; Moision, R. M.; Armentrout, P. B. *Int. J. Mass Spectrom.* **2007**, *265*, 308.
(32) Cooper, T. E.; Carl, D. R.; Armentrout, P. B. *J. Phys. Chem. A* **2009**, *113*, 13727.
(33) Carl, D. R.; Chatterjee, B. K.; Armentrout, P. B. *J. Chem. Phys.* **2010**, *132*, 044303.
(34) Cooper, T. E.; Armentrout, P. B. *Chem. Phys. Lett.* **2010**, *486*, 1.
(35) Blades, A. T.; Jayaweera, P.; Ikonomou, M. G.; Kebarle, P. *J. Chem. Phys.* **1990**, *92*, 5900.
(36) Blades, A. T.; Kebarle, P. *J. Phys. Chem. A* **2005**, *109*, 8293.
(37) Fenn, J. B.; Mann, M.; Meng, C. K.; Wong, S. F.; Whitehouse, C. M. *Mass Spectrom. Rev.* **1990**, *9*, 37.
(38) Bush, M. F.; Saykally, R. J.; Williams, E. R. *Int. J. Mass Spectrom.* **2006**, *253*, 256.
(39) Alexander, M. L.; Johnson, M. A.; Lineberger, W. C. *J. Chem. Phys.* **1985**, *82*, 5288.
(40) Alexander, M. L.; Johnson, M. A.; Levinger, N. E.; Lineberger, W. C. *Phys. Rev. Lett.* **1986**, *57*, 976.
(41) Wester, R.; Davis, A. V.; Bragg, A. E.; Neumark, D. M. *Phys. Rev. A* **2002**, *65*, 051201.
(42) Hock, C.; Schmidt, M.; Kuhnen, R.; Bartels, C.; Ma, L.; Haberland, H.; von Issendorff, B. *Phys. Rev. Lett.* **2009**, *103*, 073401.
(43) Nam, S. H.; Park, H. S.; Lee, M. A.; Cheong, N. R.; Song, J. K.; Park, S. M. *J. Chem. Phys.* **2007**, *126*, 224302.
(44) Donald, W. A.; Williams, E. R. *J. Phys. Chem. A* **2008**, *112*, 3515.
(45) Marsh, K. N. *Recommended Reference Materials for the Realization of Physiochemical Properties*; Blackwell: Oxford, U.K., 1987.
(46) Donald, W. A.; Leib, R. D.; Demireva, M.; Negru, B.; Neumark, D. M.; Williams, E. R. *J. Am. Chem. Soc.* **2010**, *132*, 6904.
(47) Yu, F. *Atmos. Chem. Phys.* **2006**, *6*, 5193.
(48) Sundén, A. E. K.; Støchkel, K.; Panja, S.; Kadhane, U.; Hvelplund, P.; Brøndsted Nielsen, S.; Zettergren, H.; Dynefors, B.; Hansen, K. *J. Chem. Phys.* **2009**, *130*, 224308.
(49) Donald, W. A.; Leib, R. D.; Demireva, M.; O'Brien, J. T.; Prell, J. S.; Williams, E. R. *J. Am. Chem. Soc.* **2009**, *131*, 13328.
(50) Donald, W. A.; Leib, R. D.; O'Brien, J. T.; Bush, M. F.; Williams, E. R. *J. Am. Chem. Soc.* **2008**, *130*, 3371.
(51) Donald, W. A.; Leib, R. D.; O'Brien, J. T.; Williams, E. R. *Chem.*—*Eur. J.* **2009**, *15*, 5926.
(52) Donald, W. A.; Williams, E. R. *J. Am. Soc. Mass Spectrom.* **2010**, *21*, 615.
(53) Holm, A. I. S.; Donald, W. A.; Hvelplund, P.; Larsen, M. K.; Nielsen, S. B.; Williams, E. R. *J. Phys. Chem. A* **2008**, *112*, 10721.

(54) Leib, R. D.; Donald, W. A.; Bush, M. F.; O'Brien, J. T.; Williams, E. R. *J. Am. Chem. Soc.* **2007**, *129*, 4894.

(55) Leib, R. D.; Donald, W. A.; Bush, M. F.; O'Brien, J. T.; Williams, E. R. *J. Am. Soc. Mass Spectrom.* **2007**, *18*, 1217.

(56) Leib, R. D.; Donald, W. A.; O'Brien, J. T.; Bush, M. F.; Williams, E. R. *J. Am. Chem. Soc.* **2007**, *129*, 7716.

(57) Prell, J. S.; O'Brien, J. T.; Holm, A. I. S.; Leib, R. D.; Donald, W. A.; Williams, E. R. *J. Am. Chem. Soc.* **2008**, *130*, 12680.

(58) O'Brien, J. T.; Prell, J. S.; Holm, A. I. S.; Williams, E. R. *J. Am. Soc. Mass Spectrom.* **2008**, *19*, 772.

(59) Holland, P. M.; Castleman, A. W., Jr. *J. Phys. Chem.* **1982**, *86*, 4181.

(60) Prell, J. S.; O'Brien, J. T.; Williams, E. R. *J. Am. Soc. Mass Spectrom.* **2010**, *21*, 800.

(61) Klots, C. E. *J. Chem. Phys.* **1985**, *83*, 5854.

(62) The bulk heat of vaporization increases from 9.7 to 10.8 kcal/mol from 373 to 273 K, and the heat of sublimation of ice is nearly constant (12.2−12.0 kcal/mol) from 273 to 130 K.

(63) Feistel, R.; Wagner, W. *J. Phys. Chem. Ref. Data* **2006**, *35*, 1021.

(64) The error bars on the figure represent the precision propagated from the noise in the mass spectra.

(65) O'Brien, J. T.; Prell, J. S.; Bush, M. F.; Williams, E. R. *J. Am. Chem. Soc.* **2010**, *132*, 8248.

(66) Rodriguez-Cruz, S. E.; Klassen, J. S.; Williams, E. R. *J. Am. Soc. Mass Spectrom.* **1999**, *10*, 958.

(67) Peslherbe, G. H.; Ladanyi, B. M.; Hynes, J. T. *J. Phys. Chem. A* **1999**, *103*, 2561.

(68) Yu, F. *J. Chem. Phys.* **2005**, *122*, 084503.

JP107547R